DYNAMIC AIRCRAFT SIMULATION MODEL COVERING LOCAL ICING EFFECTS

C. Deiler, DLR (German Aerospace Center),
Institute of Flight Systems

T. Kilian, DLR (German Aerospace Center),
Institute of Aerodynamics and Flow Technology

Lilienthalplatz 7, 38108 Braunschweig, Germany

Abstract

A novel Δ-model approach to characterize the changes in longitudinal and lateral aircraft dynamics due to local icing is analytically derived. This model extension is formulated as a separate module in the aircraft flight mechanics simulation and can be used in existing simulation models. Using the example of the former DLR research aircraft VFW 614 ATTAS, the base information about the aircraft's iced aerodynamics is obtained by 3D CFD calculations with numerically generated ice shapes. With the resulting data Δ-model parameters describing a local aerodynamic degradation are estimated. Simulation of the local ice influences on the dynamic aircraft behavior show the Δ-model's capabilities to cover aerodynamic changes during a de-icing process.

NOMENCLATURE

Symbols

a	model parameter	
α	angle of attack	rad
α_{max}	angle of attack at C_{Lmax}	rad
$C_{(\cdot)}$	aerodynamic coefficient	
c_1, $\alpha^\star$	flow separation function parameters	
D	drag force	N
d	Δ-model offset	
e	Oswald factor	
ε	downwash angle	rad
η	elevator deflection	rad
$\widehat{\eta}_{y_W^i}$	non-dimensional wing coordinate	
F	force	N
f	function	
g	acceleration due to gravity	m/s^2
H	altitude	m
i	segment index	
i_H	horizontal tail plane deflection	rad
I_{xx}, I_{yy}, I_{zz}, I_{xz}	moments of inertia	Nm^2
k	Δ-model factor	
k_1, k_2	drag coefficient factors	
L	lift force	N
Λ	wing aspect ratio	-
L, M, N	body fixed moments about x,y,z axis	Nm
l_μ	mean aerodynamic chord	m
m_{AC}	aicraft mass	kg
Ma	Mach number	
N	number of surface segments	
$\vec{\Omega}$	rotational speed vector	rad/s
P	model parameter	
p_{tot}	total pressure	N/m^2
Φ, Θ, Ψ	Euler angles	rad

p,q,r	rotational velocities	rad/s
Re	Reynolds number	
r_H, r_H^*, z_H^*	horizontal tail lever arms	m
$\vec{r}$	position vector	m
S	surface area	m^2
t	time	
T_{tot}	total temperature	°C,K
τ_2	time constant	1/s
T_b	inertia tensor	
Δt	time delay	s
u,v,w	translational velocities along x,y,z axis	m/s
V_{IAS}	indicated airspeed	m/s
V_{TAS}	true airspeed	m/s
$\vec{V}$	speed vector	m/s
$\hat{X}$	wing flow separation point	
X, Y, Z	body fixed forces along x,y,z axis	N
x, y, z	axes coordinates	

Subscripts

A	aerodynamic
b	body-fixed
Base	base model part
E	engine
H	horizontal tail
Ice	Δ-model icing part
ID	System Identification
l	rolling moment
m	pitching moment
n	yawing moment
Ref.	reference
Sim	Simulation
W	wing
WB	wing/body

Abbreviations

CFD	Computational Fluid Dynamics
LWC	Liquid Water Content
MVD	Median Volume Diameter
SLD	Supercooled Large Droplets

1 INTRODUCTION

Aerodynamic icing can have hazardous effects on aircraft performance characteristics. It can also be a limiting factor of the safe flight envelope. Icing induced dynamic behavior change and potential premature stall raise the need for pilot situational awareness and an adaption of any aircraft control strategy. During the last decades, various accidents worldwide have shown the severity of icing related degradations as well as pilot's difficulties to cope with changes in aircraft behavior [1–3]. For a better understanding of aerodynamic icing effects on aircraft performance and for enhancing future pilot training concerning icing hazards, new aerodynamic models for aircraft simulation should be developed, which is part of the HGF founded joint DLR & TU-Braunschweig research project "Supercooled Large Droplet Icing" (SulaDI).

During the flight through icing conditions, ice can accumulate on airframe parts facing the inflow e.g. wing or stabilizer leading edges, aircraft nose or engine intakes. The main aerodynamic degradation is expected to be caused by wing ice accretions and manifests itself in a reduced stall angle of attack and increased drag. These accumulations manifest in different shapes, depending on e.g. atmospheric conditions and aircraft geometry. The general aerodynamic influence is outlined for example in the "AGARD Report 344" [4] and given in Fig. 1. In the past, these effects of the icing phenomena for different airfoils and icing cases (e.g. [4–6]) as well as for complete aircraft (e.g. [7–10]) had been investigated in various studies.

From a scientific point of view different aspects of the aircraft icing phenomena are of interest. For example:

1. aircraft operational limitations and behavior with accumulated ice on different surfaces,
2. flight performance, dynamic behavior and handling quality changes during ice accretion,
3. aircraft behavior with variable accumulation severity on different surfaces,
4. aircraft behavior during de-icing and ice shedding,
5. pilot's situational awareness concerning icing and ability to detect a degradation due to ice contamination.

The challenge in describing aerodynamic degradations mathematically is to combine points 1-4 in one model formulation to extend the aerodynamics within the simulation. For dynamic simulation analysis or training in a flight simulator the model must be capable of accumulating ice on certain aircraft parts and/or de-icing the aircraft if e.g the air-

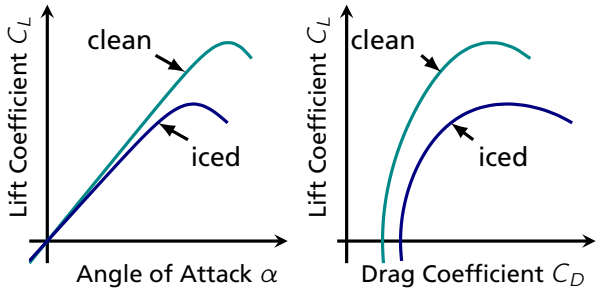

Figure 1: Expected aerodynamic degradation due to icing [4] (lift curve and drag polar)

craft leaves atmospheric icing conditions or countermeasures are activated.

This paper mainly addresses to item 1, 3 and 4 of describing the aircraft operational limitations and behavior for symmetric and asymmetric icing cases. In several attempts, the aircraft icing degradation problem had been faced based on data collected from flight test with the NASA Twin Otter at the beginning of the last decade [11–15]. With notable success, the aerodynamic model formulations had been changed and extended for reliably considering icing effects and this built-in approach was used to develop a special icing training simulator [14,16]. Another way for accounting the degradation in the simulation model is to extend an available basic aircraft model with an additional part (Δ-model in Fig. 2) in the aerodynamics module [17].

After a basic aircraft simulation model is formulated and validated for a specific aircraft, extensions for covering aerodynamic icing effects are derived to estimate and afterwards simulate performance changes. This approach gives the advantage that existing aerodynamic models do not have to be altered and the module parameters can be independently determined from the data source. Using data of flights with artificial ice shapes such an Δ-model for the fundamental effects of icing on the aircraft's longitudinal motion is presented in [18] and for all six degrees of freedom in [19].

The herein presented new Δ-model extension covers ice related changes of the longitudinal and lateral motion aerodynamics in lift, drag as well as rolling and yawing moment. Changes contributing the basic stall model formulation and the drag polar curvature are necessary to cover icing effects. The wing surface is divided into individual segments allowing the consideration of local icing effects and their consequences on the aircraft's lateral dynamics. The fundamental Δ-model formulation for icing effects is comparable to the model proposed in [11], where model parameters

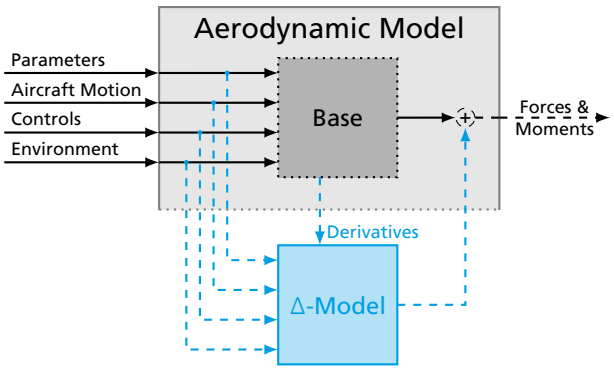

Figure 2: Illustration of aerodynamic model with Δ-model extension [18]

are linearly altered to include icing related aerodynamic degradations. To demonstrate the capability of the proposed Δ-model to reproduce aerodynamic local icing effects in the aircraft simulation, the necessary model parameters are obtained using an aerodynamics database generated by 3D CFD calculations. These calculations for the former DLR research aircraft VFW 614 ATTAS (see Fig. 3) are performed for a clean aircraft case and a case with additional attached ice shapes generated with LEWICE [20]. With the developed model the dynamic aircraft behavior during asymmetric de-icing is simulated.

2 AERODYNAMIC DATABASE OF AIRCRAFT ICING EFFECTS

A CFD study has been conducted in order to quantify the effects of leading edge icing on an aircraft's wing and horizontal tailplane (HTP) on the aerodynamic performance.

2.1 AIRCRAFT AND ICING GEOMETRY DEFINITION

The basic aircraft geometry was derived from the VFW 614 ATTAS. Its aerodynamic performance is well known and DLR pilots are well accustomed to its flight behavior. This becomes of special importance when proceeding towards an assessment

Figure 3: DLR research aircraft VFW 614 ATTAS

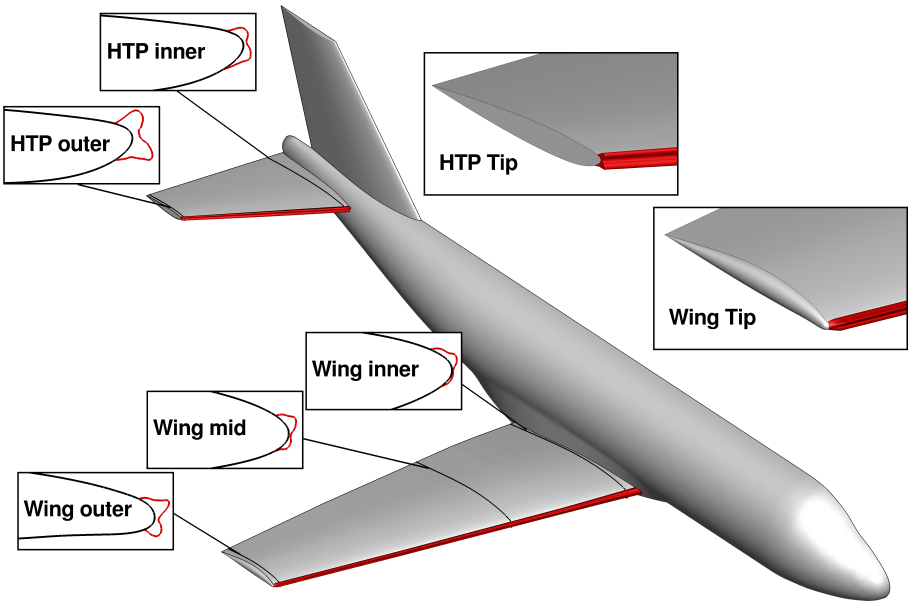

Figure 4: Overview of VFW 614 geometry with additional leading edge ice shapes

freestream velocity	V	$= 200\,\text{kt}$
		$= (103\,\text{m/s})$
total temperature	T_t	$= -10\,^\circ\text{C}$
median volume diameter	MVD	$= 119\,\mu\text{m}$
liquid water content	LWC	$= 0.7\,\text{g/m}^3$
icing time	t	$= 10\,\text{min}$
angle of attack	α	$= 2\,^\circ$

Table 1: Expected icing conditions in typical holding pattern for CFD calculations

of in-flight icing effects in a flight-simulator study. For simplification reasons and since no absolute but delta-values (iced / non-iced) are of interest, the aircraft geometry has been smoothed, cleaned of any extruding details and also the engines are neglected for CFD computations.

The leading edge ice shapes of choice had to fulfill the need for a potentially high aerodynamic impact and at the same time the corresponding icing conditions should match those of an airliner's typical holding pattern. NASA has created a public experimental database [21] of 2D Supercooled Large Droplets (SLD) ice shapes, which are known to severely influence the aerodynamic performance. Out of a set of icing conditions, which relate to a holding pattern at 200 kt, test case 7575 was chosen. It features a large leading edge horn ice shape in upward and downward direction, creating a potentially large aerodynamic performance degradation. An overview of the icing conditions is given in Tab. 1.

The chosen ice geometries were applied to the VFW 614 utilizing a technique commonly used in the process of aircraft certification: 2D ice shapes are generated on several airfoil sections of the wing and the horizontal tailplane using the icing code LEWICE, Version 2.2 [22]. A repositioning and connection of the 2D shapes results in a 3D icing structure, which can be attached to the existing clean leading edge. An overview of the iced aircraft geometry is given in Fig. 4. Section cuts illustrate the change in relative ice thickness depending on the local chord length.

2.2 NUMERICAL SETUP

Steady flow computations were performed with the TAU code, Version 2014.2, a Reynolds-averaged Navier-Stokes (RANS) solver developed by DLR [23] using unstructured hybrid meshes. Despite local flow detachments previous numerical studies on iced aircraft geometries have shown an overall steady behavior and thus proven the concept of steady computations. The two-equation Shear-Stress-Transport turbulence model (SST) by Menter [24] was applied including an extension to account for wall roughness [25].

Half-model meshes were generated with the hybrid mesh generator CENTAUR, a commercial software package developed by CentaurSoft [26]. The surface was discretized with triangles, semi-structured prism cells were stacked above to capture boundary-layer effects and the far field was filled with tetrahedral elements. The leading edge icing regions were heavily refined to capture small scale flow features. The final mesh consists of 14 million nodes for the clean and 20 million nodes for the iced case.

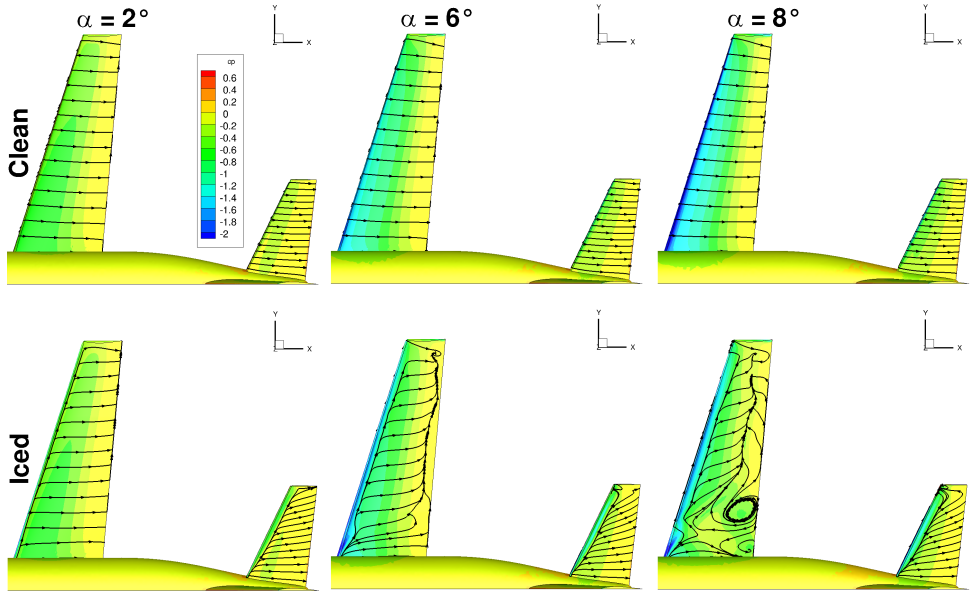

Figure 5: Surface pressure distribution and streamlines on upper wing and HTP for clean and iced configuration

2.3 DATABASE GENERATION

The simulations of the clean and iced configuration cover a wide range of angles of attack from $\alpha = -6\,^\circ$ to beyond $\alpha_{C_{L\max}}$. The boundary conditions summarized in Tab. 2 correspond to icing conditions in a holding pattern. The ice roughness was set to 3.967 mm on the wing and 2.665 mm on the HTP following an empirical correlation in [20].

Surface streamlines on the upper side of wing and HTP in Fig. 5 illustrate the gradual degradation effect leading edge icing has on the aerodynamic performance towards higher angles of attack. In the case of a clean wing the flow is fully attached throughout the depicted angle of attack regime. The iced case on the other hand shows, as expected, areas of detached flow around the leading and trailing edge at $\alpha = 6\,^\circ$ and at $\alpha = 8\,^\circ$ the wings upper surface is predominantly detached.

Mach number	Ma = 0.3
Reynolds number	Re = 21.7 million
total pressure	p_t = 88644 Pa
total temperature	T_t = 263 K

Table 2: Boundary conditions for CFD calculation

The significant icing effect on overall lift and drag coefficients is highlighted in Fig. 6. The maximum lift coefficient CL,max is reduced by 50 % from 1.2 to 0.6 and the corresponding angle of attack is reduced by 5.5 °. The zero-lift drag coefficient rises noticeably by 25 %, half of this increase can be accounted to ice roughness effects. Through the integration of local surface pressure data the spanwise distribution of forces dF/dy and moments dM/dy can be derived. The distribution of the force component in z-direction for three different angles of attack in Fig. 7 illustrates a result of this

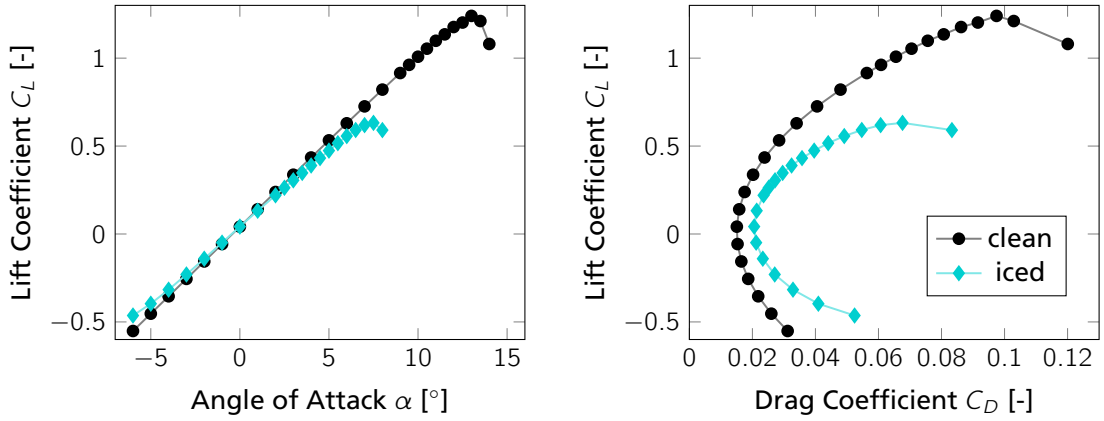

Figure 6: Coefficients of lift and drag for clean and iced configuration

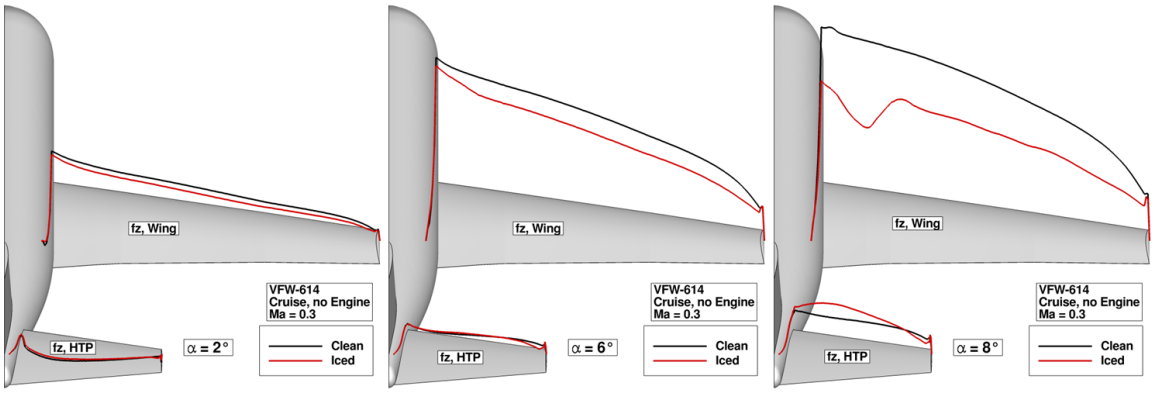

Figure 7: Spanwise distribution of local force in z-direction along wing and HTP

procedure. The implementation of icing effects into the kinematic model described in this paper is primarily based on this local evaluation of forces and moments. It allows simulation of not only symmetrical icing through mirroring the half-model but also non-symmetric conditions, e.g. through partial de-icing failure.

3 MODEL FORMULATION

The basic aircraft motion is represented by a six degree-of-freedom kinematic model. The equations of the translational motion are given by

$$\begin{aligned} \dot{u} &= -q \cdot w + r \cdot v - g \cdot \sin\Theta + \frac{X_\mathrm{E} + X_\mathrm{A}}{m_\mathrm{AC}}, \\ \dot{v} &= -r \cdot u + p \cdot w + g \cdot \cos\Theta \cdot \sin\Phi + \frac{Y_\mathrm{E} + Y_\mathrm{A}}{m_\mathrm{AC}}, \\ \dot{w} &= -p \cdot v + q \cdot u + g \cdot \cos\Theta \cdot \cos\Phi + \frac{Z_\mathrm{E} + Z_\mathrm{A}}{m_\mathrm{AC}} \end{aligned} \tag{1}$$

with the engine forces X_E, Y_E, Z_E. The unsteady nonlinear aerodynamics are modeled by the forces X_A, Y_A, Z_A in the corresponding direction. The rotational motion equations are given by

$$\begin{aligned} \begin{bmatrix} \dot{p} \\ \dot{q} \\ \dot{r} \end{bmatrix}_\mathrm{b} = T_\mathrm{b}^{-1} \left(\begin{bmatrix} L_\mathrm{E} + L_\mathrm{A} \\ M_\mathrm{E} + M_\mathrm{A} \\ N_\mathrm{E} + N_\mathrm{A} \end{bmatrix}_\mathrm{b} \right. \\ \left. - \begin{bmatrix} qr(I_{zz} - I_{yy}) - pqI_{xz} \\ rp(I_{xx} - I_{zz}) + (p^2 - r^2)I_{xz} \\ pq(I_{yy} - I_{xx}) + qrI_{xz} \end{bmatrix}_\mathrm{b} \right) \end{aligned} \tag{2}$$

including the engine induced body fixed moments L_E, M_E, N_E, the aerodynamic moments L_A, M_A, N_A, and the inverse inertia tensor

$$T_\mathrm{b}^{-1} = \begin{bmatrix} I_{xx} & 0 & -I_{xz} \\ 0 & I_{yy} & 0 \\ -I_{xz} & 0 & I_{zz} \end{bmatrix}_\mathrm{b}^{-1}. \tag{3}$$

The necessary forces and moments for the aircraft motion simulation result form the base aircraft aerodynamic model (section 3.1) and additional Δ-model formulation in section 3.2.

3.1 BASE AIRCRAFT AERODYNAMICS

The base aircraft aerodynamic model is formulated as a two-point model, splitting wing and horizontal tailplane influences (see Fig. 8). For the wing aerodynamics, a nonlinear,unsteady lift curve is considered, which allows to simulate flow separation and reattachment effects [28]. The complete aerodynamic model of the VFW 614 ATTAS is given in [29] as a system identification process result. Several equations of the longitudinal aerodynamics model are outlined hereafter as a basis for the later on derived Δ-model formulation. The lateral aerodynamics model formulation – a state of the art derivative model – can be found in [29]. Furthermore, the base aircraft model formulation similar to the herein used ATTAS-model is outlined in [18, 19], where comparable approaches to account for icing effects in the dynamic simulation are presented.

The non-dimensional steady wing flow separation point $\widehat{X}$ is given by [30]

$$\widehat{X} = \frac{1}{2} \cdot \left(1 - \tanh\left(c_1 \cdot (\alpha - \alpha^\star)\right)\right), \tag{4}$$

whereas $\alpha^\star$ denotes the angle of attack for which the wing flow is half separated. The simplified wing/body lift coefficient equation including stall – considering Kirchhoff's theory of flow separation from the trailing edge – results in

$$C_{L,\mathrm{WB}} = C_{L0} + C_{L\alpha,\mathrm{WB}} \cdot \left(\frac{1 + \sqrt{\widehat{X}}}{2}\right)^2 \alpha. \tag{5}$$

The basic drag equation is dominated by zero, lift induced and stall dependent drag and can be expressed by

$$C_D = C_{D0} + \frac{1}{e\pi\Lambda} C_{L+}^2 \frac{\partial C_D}{\partial \widehat{X}} \left(1 - \widehat{X}\right). \tag{6}$$

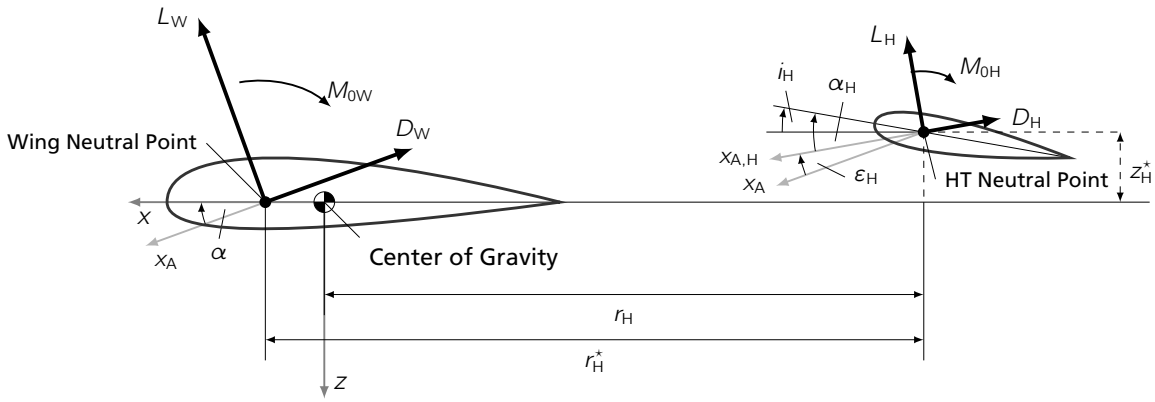

Figure 8: Illustration wing and horizontal tail geometry for the two-point model formulation [27]

3.2 Δ-MODEL EXTENSION

The necessary equations to implement a Δ-model approach (as given in Fig. 2) to consider local icing effects are derived hereafter. The basic idea is to use linear altered parameters for icing induced aerodynamic changes in aircraft simulation, which was introduced by Bragg [11]. Hence, a model parameter P is assumed to consist of a basic model part P_{Base} and an additional Δ-model part ΔP_{Ice} describing the icing induced changes:

$$P = (1 + k_P) \cdot P_{\text{Base}} + d_P = P_{\text{Base}} + \Delta P_{\text{Ice}} \tag{7}$$

The additional factor k_P and the offset d_P are used to model the degraded aircraft aerodynamics. As a result, an aerodynamic model coefficient $C_{(\cdot)}$ which depends on an extended parameter P can be expressed as:

$$\begin{aligned} C_{(\cdot)}(P) &= C_{(\cdot)}\left(P_{\text{Base}} + \Delta P_{\text{Ice}}\right) \\ &= \left(C_{(\cdot)}\left(P_{\text{Base}}\right)\right)_{\text{Base}} \\ &\quad + \Delta\left(C_{(\cdot)}\left(P_{\text{Base}} + \Delta P_{\text{Ice}}\right)\right)_{\text{Ice}}. \end{aligned} \tag{8}$$

At this stage of model development only the icing influence on the aircraft's wing is considered.

3.3 LOCAL WING SEGMENT EQUATIONS

The aircraft wing is divided span-wise in N segments with the same wing segment width y_W^i but consequently different cord length and surface area. This segmentation is shown for example in Fig. 9 for $N = 20$ segments.

With the distance vector $\vec{r}^{\,i}$ of the ith segment to CG the local segment inflow velocities (without wind) are given by

$$\begin{aligned} &\vec{V}^{\star i} = \vec{V} + \vec{\Omega} \times \vec{r}^{\,i}, \\ &\text{with} \quad \vec{V}^{\star i} = \left[u^{\star i}, v^{\star i}, w^{\star i}\right]^T, \ \vec{\Omega}^{\,i} = [p, q, r]^T \\ &\text{and} \quad \vec{r}^{\,i} = \left[x_{\text{W,CG}}^i, y_{\text{W,CG}}^i, y_{\text{W,CG}}^i\right]^T. \end{aligned} \tag{9}$$

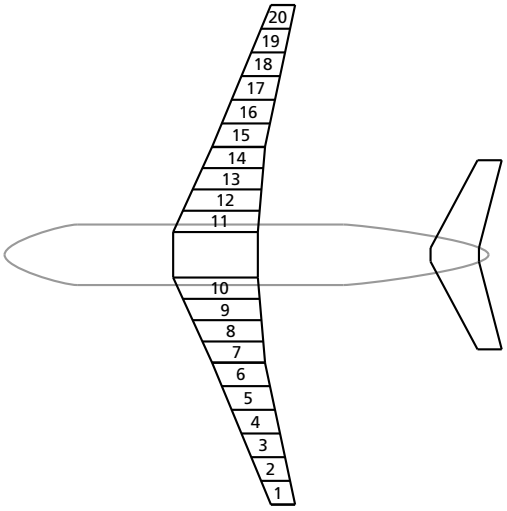

Figure 9: Illustration of Δ-model wing segmentation ($N = 20$)

Considering modern aircraft's swept angle φ and dihedral ν the local velocities $u^{\star i}$, $v^{\star i}$ and $w^{\star i}$ result in u^i, v^i and w^i, which are the local inflow velocities rectangular to the local 25 % chord line. With the local true airspeed

$$V_{\text{TAS}}^i = \sqrt{\left(u^i\right)^2 + \left(v^i\right)^2 + \left(w^i\right)^2} \tag{10}$$

the local angle of attack of the i-th segment results in

$$\alpha^i = \arctan\left(\frac{w^i}{u^i}\right). \tag{11}$$

To determine the aerodynamic influence of each Δ-model segment, an additional lift and drag coefficient as a local change towards the base aircraft aerodynamic is calculated. The changes of the lateral aerodynamics further result from the summation of all these segments influences and their corresponding lever arms $\left(\vec{r}^{\,i}\right)$. The following equations are the results of splitting the aerodynamic model formulations in [29] into their base and icing parts using the parameter extension according to equation (8).

With the extension given in equation (7), the parameters of the non-dimensional separation point without hysteresis effects according to [30]

$$\begin{aligned} c_1^i &= \left(1 + k_{c_1}^i\right) \cdot c_{1\,\mathrm{Base}} \\ \alpha^{\star i} &= \left(1 + k_{\alpha^\star}^i\right) \cdot \alpha^\star{}_{\mathrm{Base}} \end{aligned} \tag{12}$$

lead to a separation of the hyperbolic tangens term of each segment i into its base part

$$a_{1\mathrm{Base}}^i = c_{1\mathrm{Base}} \cdot \left(\alpha^i - \alpha^\star\right) \tag{13}$$

and its icing induced part

$$a_{1\mathrm{Ice}}^i = c_{1\mathrm{Base}} \cdot \left[k_{c_1}^i \alpha - \alpha^\star \left(k_{c_1}^i + k_{\alpha^\star}^i \left(1 + k_{c_1}^i\right)\right)\right]. \tag{14}$$

This analytic separation results in the local non-dimensional flow separation point of the base aircraft

$$\widehat{X}_{\mathrm{Base}}^i = 0.5 \cdot \left(1 - \tanh(a_{1\mathrm{Base}}^i)\right) \tag{15}$$

and its icing induced adaption $\Delta\widehat{X}_{\mathrm{Ice}}^i$

$$\Delta\widehat{X}_{\mathrm{Ice}}^i = \frac{\tanh(a_{1\mathrm{Ice}}^i) - \tanh^2(a_{1\mathrm{Base}}^i)\tanh(a_{1\mathrm{Ice}}^i)}{-2 \cdot \left(1 + \tanh(a_{1\mathrm{Base}}^i)\tanh(a_{1\mathrm{Ice}}^i)\right)}. \tag{16}$$

With the parameter extensions for the i-th segment

$$\begin{aligned} C_{L0}^i &= \left(1 + k_{C_{L0}}^i\right) \cdot C_{L0\,\mathrm{Base}} \\ C_{L\alpha,\mathrm{WB}}^i &= \left(1 + k_{C_{L\alpha,\mathrm{WB}}}^i\right) \cdot C_{L\alpha,\mathrm{WB\,Base}} \end{aligned} \tag{17}$$

and the separated influences of the local flow separation

$$a_{2\mathrm{Base}}^i = 0.25 \cdot \left(1 + 2\sqrt{\widehat{X}_{\mathrm{Base}}^i} + \widehat{X}_{\mathrm{Base}}^i\right) \tag{18}$$

$$\begin{aligned} a_{2\mathrm{Ice}}^i = 0.25 \cdot \Bigg(&2\sqrt{\widehat{X}_{\mathrm{Base}}^i + \Delta\widehat{X}_{\mathrm{Ice}}^i} \\ &- 2\sqrt{\widehat{X}_{\mathrm{Base}}^i} + \Delta\widehat{X}_{\mathrm{Ice}}^i\Bigg) \end{aligned} \tag{19}$$

the local lift coefficient change $\Delta C_{L,\mathrm{WB\,Ice}}^{\star i}$ results in

$$\begin{aligned} \Delta C_{L,\mathrm{WB\,Ice}}^{\star i} = \;& k_{C_{L0}}^i C_{L0\,\mathrm{Base}} \\ &+ (a_{2\mathrm{Base}}^i + a_{2\mathrm{Ice}}^i) k_{C_{L\alpha,\mathrm{WB}}}^i C_{L\alpha,\mathrm{WB\,Base}} \alpha^i \\ &+ a_{2\mathrm{Ice}}^i C_{L\alpha,\mathrm{WB\,Base}} \alpha^i. \end{aligned} \tag{20}$$

This coefficient change is related to each segment's wing surface area S_{W}^i. Consequently the local lift coefficient change $\Delta C_{L,\mathrm{WB\,Ice}}^{\star i}$ must be transferred to a general value $\Delta C_{L,\mathrm{WB\,Ice}}^i$ by

$$\Delta C_{L,\mathrm{WB\,Ice}}^i = \Delta C_{L,\mathrm{WB\,Ice}}^{\star i} \frac{S_{\mathrm{W}}^i}{S_{\mathrm{W}}}. \tag{21}$$

To calculate the local drag coefficient change necessitates to approximate the local change of

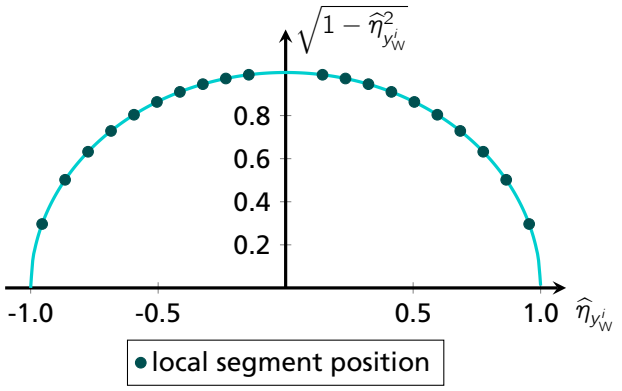

Figure 10: Elliptic distribution including the spanwise positions of 20 wing segments

the lift induced drag for each segment. An elliptic wing lift distribution based on the non-dimensional wing coordinate

$$\widehat{\eta}_{y_{\mathrm{W}}^i} = \frac{y_{\mathrm{W}}^i}{s} \tag{22}$$

of each segment is assumed for the base aircraft aerodynamics (see Fig. 10). The local base lift coefficient $C_{L,\mathrm{WB\,Base}}^{\star i}$ is approximated as a function of the general base lift coefficient, local and complete wing surface area and the non-dimensional wing coordinate $\widehat{\eta}_{y_{\mathrm{W}}^i}$:

$$C_{L,\mathrm{WB\,Base}}^{\star i} = f\left(C_{L,\mathrm{WB\,Base}}, S_{\mathrm{W}}, \widehat{\eta}_{y_{\mathrm{W}}^i}, S_{\mathrm{W}}^i\right) \tag{23}$$

Hence, the local ice induced drag coefficient change is formulated as

$$\begin{aligned} \Delta C_{D,\mathrm{WB\,Ice}}^{\star i} = \;& k_{C_{D0}}^i C_{D0\,\mathrm{Base}} \\ &+ \Delta C_{L,\mathrm{WB\,Ice}}^{\star i\,2} \frac{1}{e\pi\Lambda} \\ &+ 2 \cdot \Delta C_{L,\mathrm{WB\,Ice}}^{\star i} C_{L,\mathrm{WB\,Base}}^{\star i} \frac{1}{e\pi\Lambda} \\ &+ \left(\Delta C_{L,\mathrm{WB\,Ice}}^{\star i} + C_{L,\mathrm{WB\,Base}}^{\star i}\right) \cdot d_{k_1}^i \\ &+ \left(\Delta C_{L,\mathrm{WB\,Ice}}^{\star i} + C_{L,\mathrm{WB\,Base}}^{\star i}\right)^2 \cdot \frac{k_{k_2}^i}{e\pi\Lambda} \\ &+ k_{\frac{\partial C_D}{\partial \widehat{X}}}^i \frac{\partial C_D}{\partial \widehat{X}} \left(1 - \left(\widehat{X}_{\mathrm{Base}}^i + \Delta\widehat{X}_{\mathrm{Ice}}^i\right)\right) \\ &- \frac{\partial C_D}{\partial \widehat{X}} \Delta\widehat{X}_{\mathrm{Ice}}^i \end{aligned} \tag{24}$$

using the parameter extensions

$$\begin{aligned} C_{D0}^i &= \left(1 + k_{C_{D0}}^i\right) \cdot C_{D0\,\mathrm{Base}} \\ k_2^i &= \frac{\left(1 + k_{k_2}^i\right)}{e\pi\Lambda} \\ \left(\frac{\partial C_D}{\partial \widehat{X}}\right)^i &= \left(1 + k_{\frac{\partial C_D}{\partial \widehat{X}}}^i\right) \cdot \frac{\partial C_D}{\partial \widehat{X}}_{\mathrm{Base}}, \end{aligned} \tag{25}$$

The linear lift depended drag coefficient is introduced in the Δ-model as an offset $d_{k_1}^i$, because

there is no part of the base model which could be linear extended. The general additional segment drag coefficient $\Delta C^i_{D,\mathrm{WB_{Ice}}}$ can be calculated analog equation (21). The local force coefficients result from $\Delta C^i_{X,\mathrm{W_{Ice}}}$ and $\Delta C^i_{Z,\mathrm{W_{Ice}}}$ result from equations (21) and (24) by turning the aerodynamic coefficients around the local angle of attack α^i

$$\begin{aligned} \Delta C^i_{X,\mathrm{W_{Ice}}} &= \quad \Delta C^i_{L\,\mathrm{Ice}} \sin\left(\alpha^i\right) - \Delta C^i_{D\mathrm{Ice}} \cos\left(\alpha^i\right) \\ \Delta C^i_{Z,\mathrm{W_{Ice}}} &= -\Delta C^i_{L\,\mathrm{Ice}} \cos\left(\alpha^i\right) - \Delta C^i_{D\mathrm{Ice}} \sin\left(\alpha^i\right). \end{aligned} \tag{26}$$

Further the rolling and yawing moment contributions of the i-th wing segment are given by

$$\begin{aligned} \Delta C^i_{l,\mathrm{W_{Ice}}} &= \quad \Delta C^i_{Z,\mathrm{W_{Ice}}} \cdot \frac{y^i_{\mathrm{W}}}{s} \\ \Delta C^i_{n,\mathrm{W_{Ice}}} &= -\Delta C^i_{X,\mathrm{W_{Ice}}} \cdot \frac{y^i_{\mathrm{W}}}{s}. \end{aligned} \tag{27}$$

In this version of the Δ-model, no wing pitching moment or side force change is considered, but could also be added by suitable model formulations. It is assumed that the aerodynamics changes introduced by the herein presented Δ-model cover the primary icing effects on aircraft dynamics.

3.4 GLOBAL ICING INFLUENCE

The above derived equations to determine the local icing induced aerodynamic changes in a dynamic aircraft simulation model allow to calculate the new global force coefficients by summing up the influence of each segment i. The new force coefficient result in

$$\begin{aligned} C_X &= C_{X\,\mathrm{Base}} + \sum_i \Delta C^i_{X,\mathrm{W_{Ice}}} \\ C_Z &= C_{Z\,\mathrm{Base}} + \sum_i \Delta C^i_{Z,\mathrm{W_{Ice}}}, \end{aligned} \tag{28}$$

and the new moment coefficients are given by

$$\begin{aligned} C_l &= C_{l\,\mathrm{Base}} + \sum_i \Delta C^i_{l,\mathrm{W_{Ice}}} \\ C_n &= C_{n\,\mathrm{Base}} + \sum_i \Delta C^i_{n,\mathrm{W_{Ice}}}. \end{aligned} \tag{29}$$

4 Δ-MODEL PARAMETER ESTIMATION

The parameters of the above derived Δ-model are obtained from the CFD results in section 2 by an automated process using system identification techniques. First, the lift and drag coefficients of each wing segment are calculated by summing up the n local discrete forces $F_{X,n}$ and $F_{Z,n}$ given by

Separation:	$\alpha^{\star i}$	c^i_1		
Lift:	C^i_{L0}	$C^i_{L\alpha,\mathrm{WB}}$		
Drag:	C^i_{D0}	k^i_1	k^i_2	$\left(\frac{\partial C_D}{\partial \widehat{X}}\right)^i$

Table 3: Estimated parameters of the local segment reference aerodynamics

the force distributions dF/dy for the different angles of attack:

$$\begin{aligned} C^i_{D,\mathrm{CFD}}(\alpha) &= \sum_n \frac{\left(\quad F_{X,n}\cos(\alpha) + F_{Z,n}\sin(\alpha)\right)}{\overline{q} S^i_{\mathrm{W}}} \\ C^i_{L,\mathrm{CFD}}(\alpha) &= \sum_n \frac{\left(-F_{X,n}\sin(\alpha) + F_{Z,n}\cos(\alpha)\right)}{\overline{q} S^i_{\mathrm{W}}} \end{aligned} \tag{30}$$

The necessary information for the parameter estimation is available[1] after the application of equation (30) to the clean aircraft and iced CFD data. Before the Δ-model parameters can be estimated, corresponding base model parameters for each strip are needed. Using these parameters, the formulations derived in section 3.3 can be applied on the iced aircraft CFD results. Therefore a nonlinear regression technique to determine the base aircraft lift and drag coefficients is performed, using a model formulation similar to the equations in section 3.1, with initial parameter values for zero lift, lift slope, zero lift drag and lift dependent drag previously obtained by a simple linear regression. For the nonlinear regression the DLR Matlab® toolbox Fitlab [31] is used, providing a set of algorithms to optimize model parameters in different domains. The corresponding base model segment parameters are listed in Tab. 3. These parameters are segment related and therefore comparable to the e. g. lift coefficient in equation (23).

With the base segment model available, the desired local wing segment Δ-model parameters are estimated also by using a nonlinear regression technique. The resulting fit of lift and drag coefficient is shown in Fig. 11 for one example wing segment.

The CFD results are well matched using the base model formulation. Furthermore, the combination of base and Δ-model to cover the icing degradation does not show significant deviations from the CFD results. Consequently it is assumed, that the Δ-model structure and its parameter estimates reliably cover the aerodynamic changes of each wing segment due to ice accretion. The local segment coefficients are related to the complete wing surface area (see for example equation (21)), which

[1] Note that the data are clipped for further processing to an angle of attack range without unreliable post-stall behavior

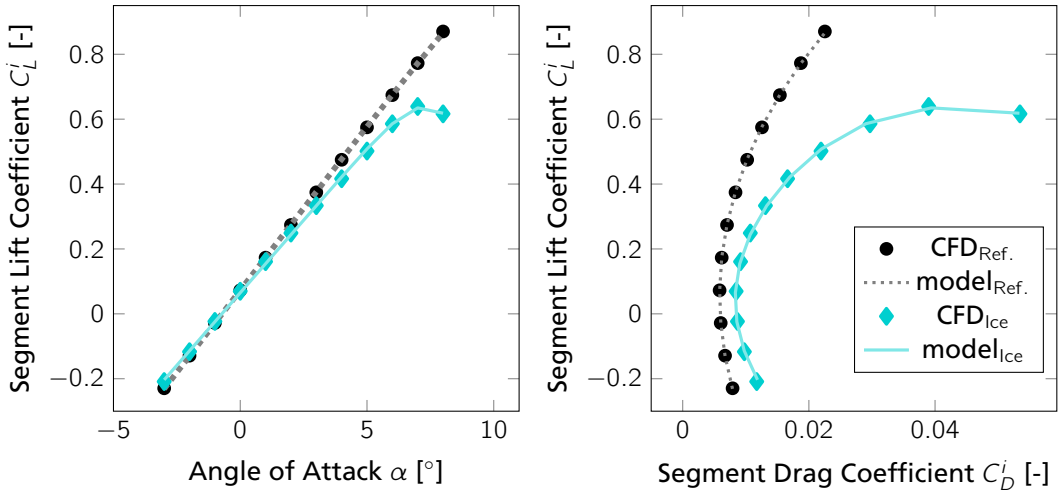

Figure 11: Comparision of wing segment lift and drag coefficient, $i = 6$, $N = 20$

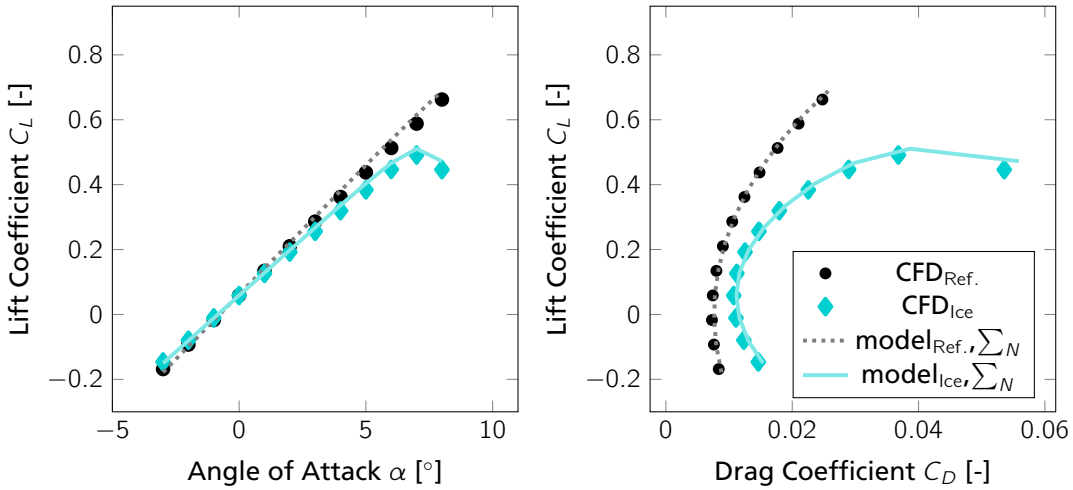

Figure 12: Comparision of complete aircraft lift and drag coefficient, $N = 20$

allows the direct summation of all individual wing segment Δ model results to the complete icing influence. Figure 12 shows a comparison of lift and drag curves for local summed influences (after parameter estimation) and complete aircraft CFD results. The good matches of the results indicate that the proposed method to cover local aerodynamic icing effects is well applicable.

The final step is to transfer the obtained Δ-model parameter estimates to values usable in the ATTAS simulation model. The available simulation model identified from flight data contains different parameter values than the parameter estimates obtained for the clean basic model from the CFD results. These results are calculated without engine pylons, which have an influence on the wing flow and consequently on the complete aircraft drag. Therefore the herein estimated Δ-model parameters are linearly transformed for the usages with the identified aircraft model. The corresponding segment parameter estimates of the Δ-model ($N = 20$ wing segments) are given in Tab. 5.

5 LOCAL ICING INFLUENCE ON AIRCRAFT BEHAVIOR

For the aircraft simulation it is suitable to allow a fading between the base aircraft and the icing degradation, instead of suddenly switching on the icing influence. An additional fading factor k_{Ice}^i, which describes the icing severity [11], is used to scale each segment's Δ-model parameters during the simulation:

$$k_{(\cdot),\text{Sim}}^i(t) = k_{\text{Ice}}^i(t) \cdot k_{(\cdot)}^i. \tag{31}$$

If k_{Ice}^i is set to zero for all segments, the aircraft behavior is only influenced by the base aerodynamics. For all other values of k_{Ice}^i, the aircraft's aerodynamic behavior is degraded due to the icing effects activated in the simulation by the Δ-model. This allows to simulate ice accretion by slowly increasing k_{Ice}^i as well as de-icing using a sudden k_{Ice}^i decrease. The changes in lift curve and drag polar between the base and icing degraded aircraft for different values of k_{Ice}^{1-20} (symmetric ice case) is

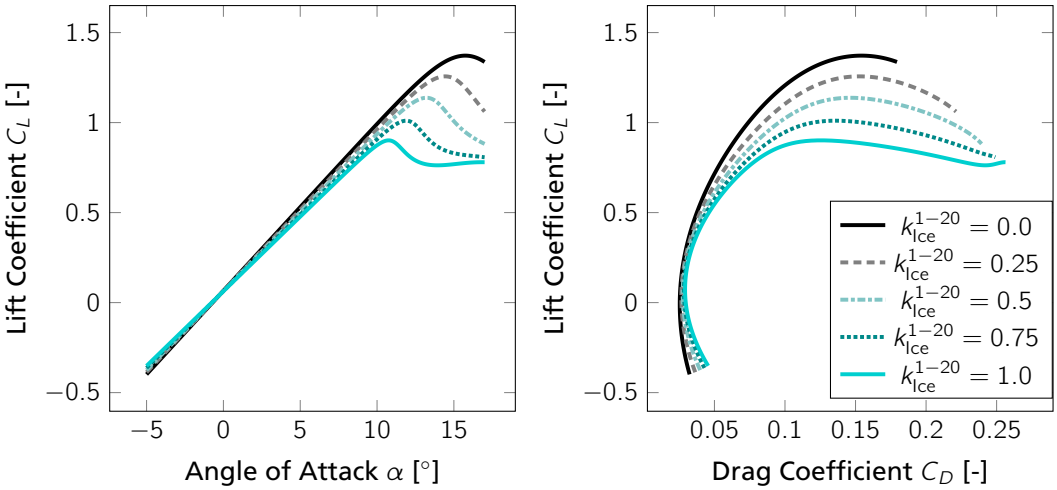

Figure 13: Adaption of ATTAS aerodynamic characteristics for wing icing by the Δ-model ($N = 20$)

given in Fig. 13, using the transfered segment parameters given in Tab. 5.

The herein developed Δ-model provides the capability to only degrade the aerodynamics of certain wing parts represented by the individual segments. This provides the possibility to simulate asymmetric icing effects on an aircraft's dynamic motion. To demonstrate this capability, the aerodynamic model is evaluated for different angles of attack between $-5\,°$ and $17\,°$ and a flight in 10000 ft with Mach 0.3, which corresponds to the case used for the CFD calculation.

The additional rolling moment coefficient $\Delta C^i_{l,\text{W}_{\text{Ice}}}$ generated by each segment $i \in [11, 20]$ ($k^i_{\text{Ice}} = 1.0$, $k^{1-10}_{\text{Ice}} = 0.0$) on the right wing are given in Fig. 14 to analyze each wing segment's degrading influence on the lateral aircraft aerodynamics. The maximum rolling influence for high angles of attack $\alpha > 12\,°$ result from segments #17 and #18 in Fig. 9. The significant lift degradation for these segments in combination with the large lever arm cause the large rolling moments. The additional rolling moments of segments #19 and #20 are smaller because of the smaller corresponding lift degradation due to small segment surfaces. For angles of attack between 0° and 10° the outer segments show the strongest influence because the large lever arms and the gradual degrading effects of the wing span. Similar results are obtained for the individual yawing moment coefficient $\Delta C^i_{n,\text{W}_{\text{Ice}}}$ of each right wing segment given in Fig. 14. For lower angles of attack up to 10°, the outer wing segments gradually influence the additional yawing moment. But with $\alpha > 10°$ the segments #17 and #18 show the most significant effect because of the combination of drag increase and large lever arm.

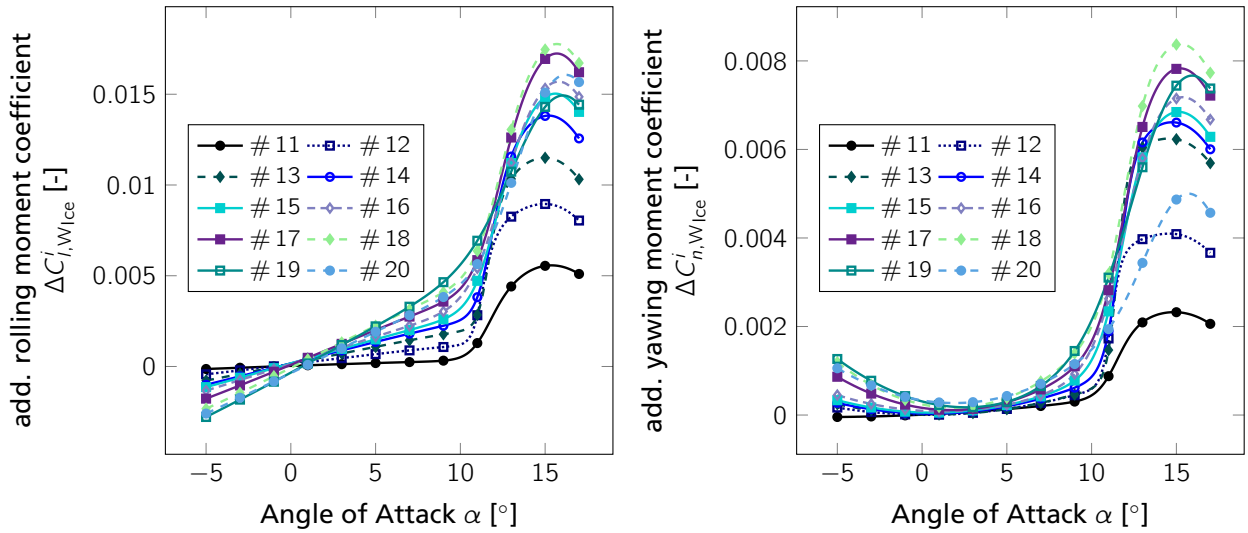

Figure 14: Additional single rolling and yawing moment coefficients due to individually iced right wing segments ($k^{1-10}_{\text{Ice}} = 0.0$, $N = 20$)

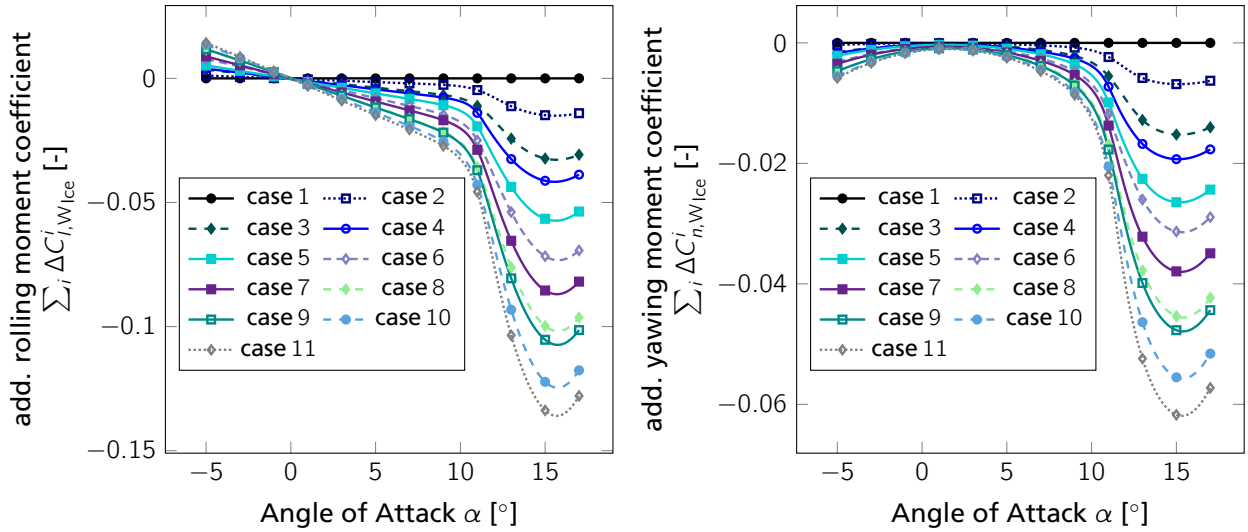

Figure 15: Additional complete rolling and yawing moment coefficients due to several iced/ de-iced right wing segments ($k^{1-10}_{\mathrm{Ice}} = 1.0$)

case	k^{11}_{Ice}	k^{12}_{Ice}	k^{13}_{Ice}	k^{14}_{Ice}	k^{15}_{Ice}	k^{16}_{Ice}	k^{17}_{Ice}	k^{18}_{Ice}	k^{19}_{Ice}	k^{20}_{Ice}
1	1	1	1	1	1	1	1	1	1	1
2	1	1	1	1	0	1	1	1	1	1
3	1	1	1	1	0	1	1	0	1	1
4	1	0	1	1	0	1	1	0	1	1
5	1	0	1	1	0	0	1	0	1	1
6	1	0	1	1	0	0	1	0	1	0
7	1	0	1	0	0	0	1	0	1	0
8	1	0	1	0	0	0	1	0	0	0
9	0	0	1	0	0	0	1	0	0	0
10	0	0	1	0	0	0	0	0	0	0
11	0	0	0	0	0	0	0	0	0	0

Table 4: Example random de-icing pattern for right wing segments

To further demonstrate the model's capability of covering asymmetric icing effects, model simulation results including variable segment icing severity are provided. In Tab. 4 a set of 11 cases is given describing a random de-icing pattern for the right wing segments, which is similar to a distinct activation of certain de-icing installations (like electro impuls de-icing [32]), whereas the left wing stays contaminated ($k^{1-10}_{\mathrm{Ice}} = 1.0$). This could be seen as a left side de-icing system malfunction. The first case contains a complete iced wing ($k^{11-20}_{\mathrm{Ice}} = 1.0$) and case 11 a fully de-iced right wing ($k^{11-20}_{\mathrm{Ice}} = 0.0$). The additional rolling moment coefficient as a sum of each segments individual influence is given in Fig. 15 versus the angle of attack. Because of the de-icing cases all moments are opposed to the individual moment coefficients in Fig. 14. Similar to the individual icing analysis the influence increases with the angle of attack and beginning wing separation. With all right wing segments de-iced the additional rolling moment $\sum_i \Delta C^i_{l,\mathrm{W_{Ice}}}$ also shows a strong increase of icing influence over $10°$ and reaches almost a value of -0.136 at an angle of attack of $15°$, which corresponds to about $118\,\%$ of the clean aircraft roll control authority. Hence, the aircraft would be uncontrollable in that case. Comparable results are obtained for the additional yawing moments coefficient $\sum_i \Delta C^i_{n,\mathrm{W_{Ice}}}$, which reaches a maximum value of about -0.062 for the asymmetric ice case ($k^{11-20}_{\mathrm{Ice}} = 0.0$) at $\alpha = 15°$.

Using the in Tab. 4 given pattern for the right wing, the aircraft motion for an asymmetric wing de-icing case can be simulated with the developed model. The pattern is therefore transfered to a de-icing command for each individual segment i, changing the corresponding state of the severity factor k^i_{Ice} linearly from 1 to 0 within $0.2\,\mathrm{s}$. After one segment is fully de-iced the process is triggered for the next segment according to the predefined pattern. To demonstrate these model capabilities a de-icing example case beginning with a trimmed steady horizontal flight in $10000\,\mathrm{ft}$ with an indicated airspeed of $160\,\mathrm{kt}$ is simulated, with the de-icing process starting after $6\,\mathrm{s}$ of simulation time. The resulting time histories of several aircraft states and outputs are given in Fig. 16 illustrating the aircraft's behavior during and after the right wing is de-iced. No counteracting pilot inputs are applied, which results in an uncontrolled flight after the aircraft is asymmetrically de-iced. The de-icing starts with segment $\#15$, which is located in the mid part of the wing, followed by the further outboard segment $\#18$. The aircraft starts to roll

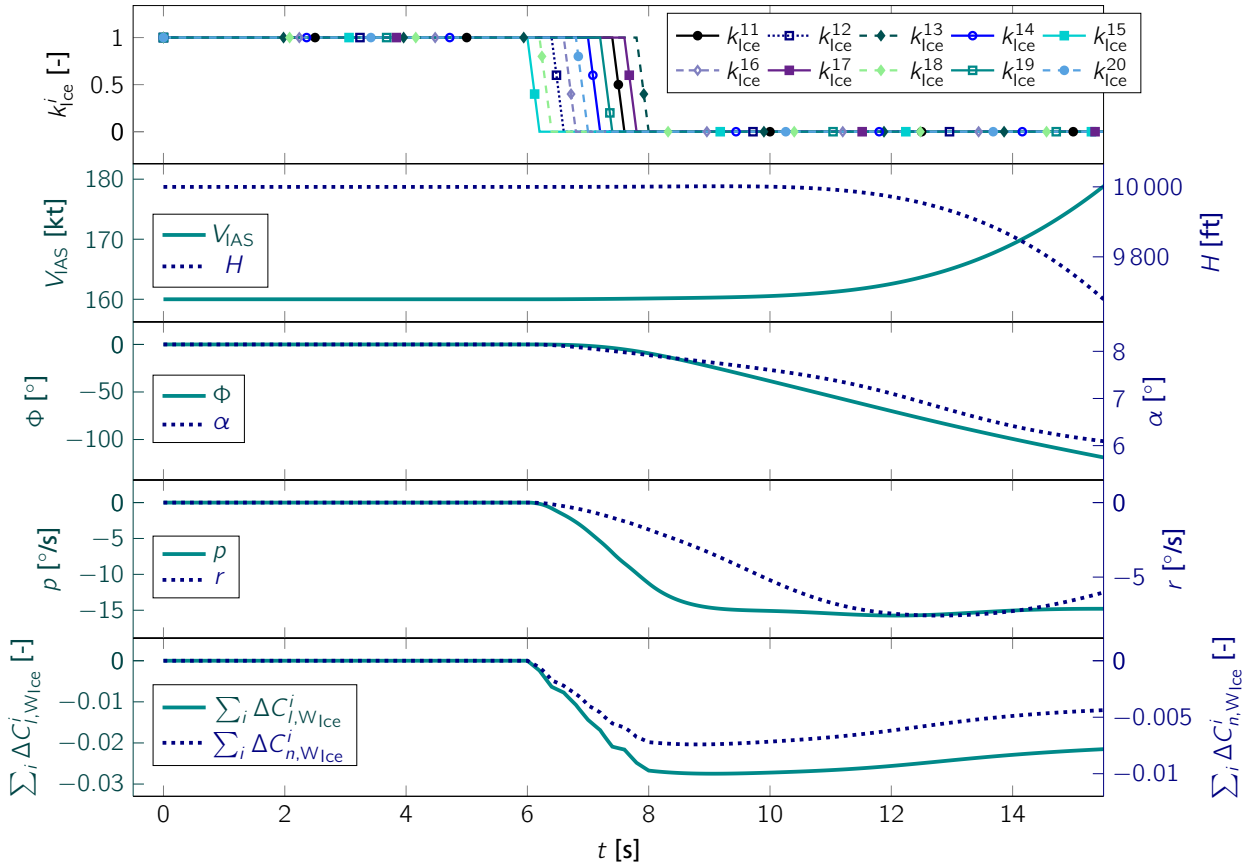

Figure 16: Dynamic aircraft behavior for right wing de-icing with random pattern ($k^{1-10}_{\mathrm{Ice}} = 1.0$)

and yaw to the left resulting in a spiral motion. With all segments de-iced the aircraft's rolling rate exceeds $15°/\mathrm{s}$ and due to the spiral motion the airspeed increases with a loss of altitude.

According to Fig. 14 each segment has a different influence on the lateral moments and hence resulting aircraft motion, which also manifests in the dynamic aircraft simulation. A detailed time history plot of the resulting additional lateral moments and the rotational accelerations $\dot{p}$ & $\dot{r}$ for the simulated de-icing process between $t = 6$ and $8\,\mathrm{s}$ is given in Fig. 17. Depending on the position and the aerodynamic influence of each segment, the resulting contribution to the additional lateral moments is different during de-icing. The inboard segments $\#\,11$ to $\#\,14$ have a small additional influence on the rolling motion at medium angles of attack – as given in Fig. 14 – which means, that the additional rolling moment caused by the de-icing is also small. The removal of the ice influence of segment $\#\,12$ beginning at $6.4\,\mathrm{s}$ or segment $\#\,11$ beginning at $7.4\,\mathrm{s}$ results in only a small additional value of $\Delta C^i_{l,\mathrm{WIce}}$. During the de-icing of segment $\#\,12$, the roll damping influence of the wing dominates the roll acceleration and eliminates the additional de-icing influence. For de-icing of segment $\#\,11$, the damping influence exceeds the additional roll influences, and the aircraft's roll acceleration is reduced. In contrast, the removal of the ice influence at the outboard segment $\#\,19$ at $t = 7.2\,\mathrm{s}$ significantly increases the roll acceleration although the aircraft encounters a large roll damping influence due to the established rolling motion. A similar behavior with reduced effects is visible for the yaw influence given also in Fig. 17.

With these first results, it can be stated, that the new Δ-model formulation allows to reliably account for local wing icing effects and consequently the behavior during and after icing removal.

6 CONCLUSION

In this paper a methodology to formulate the local degrading effects of icing on aircraft aerodynamics in a dynamic simulation is presented. The developed Δ-model formulation allows to use an arbitrary number of segments distributed over the complete wing span which are individually responsible for the local aerodynamic degradation. With information of the iced aerodynamics available through various different sources, the corresponding model parameters of each segment can be determined.

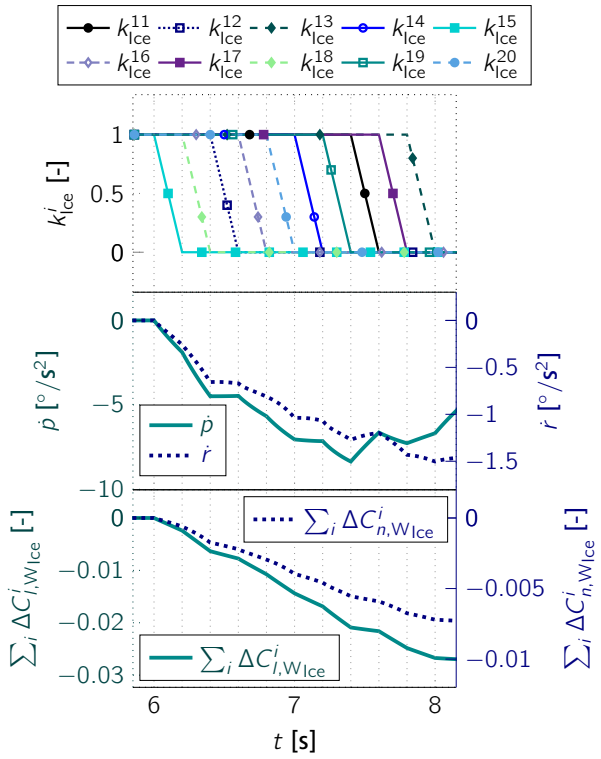

Figure 17: Additional lateral moments during right wing de-icing with random pattern ($k_{\mathrm{Ice}}^{1-10} = 1.0$, detailed plot of Fig. 16)

In the given example, the Δ-model is used to account for icing effects on the former DLR research aircraft VFW 614 ATTAS. The results of CFD calculations of a three-dimensional ATTAS aircraft geometry with and without attached ice shapes are the base for the Δ-model parameter estimation. With the resulting new aerodynamic model the aircraft behavior for different icing cases was evaluated. The simulation of an asymmetric de-icing case where a random pattern is used to segment-wise remove the right wing degradation shows the model capabilities and allows to evaluate the aircraft behavior in this special case as a first result.

With the herein developed model further evaluations concerning the flight performance, flight dynamic changes, altered handling qualities will be conducted. Also an additional formulation for the degradation of the horizontal tailplane will be developed similar to the wing Δ-model and degrading effects of icing on control surfaces will be taken into account to analyze the aircraft controllability. New results of CFD calculation for different ice shapes – generated with the new DLR icing code TAUICE [33] – attached to the ATTAS aircraft will result in different parameter sets and therefore further analysis. Hence, the differences between ice shapes with distinct degrading aerodynamic influences on the aircraft will be evaluated.

References

[1] Bundesstelle für Flugunfalluntersuchung, *Final Report (BFU 5X011-0/98)*. April, 2001, Braunschweig, DE.

[2] Green, Steven D.: *A Study of U. S. Inflight Icing Accidents and Incidents, 1978 to 2002*. 44th AIAA Aerospace Sciences Meeting and Exhibit, Reno, Nevada, USA, January 9th - 12th, 2006. American Institute of Aeronautics and Astronautics, Inc. (AIAA), Paper No. AIAA 2006-82.

[3] National Transportation Safety Board (NTSB), *Aircraft Accident Report (NTSB/AAR-96/01, DCA95MA001), Safety Board Report*. July 9th, 1996, Washington, DC, USA.

[4] Advisory Group for Aerospace Research & Development (AGARD): *Ice Accretion Simulation*. AGARD Advisory Report 344, Fluid Dynamics Panel Working Group 20, North Atlantic Treaty Organization (NATO), Neuilly-Sur-Seine, France, December, 1997.

[5] Gray, Vernon H.: *Prediction of aerodynamic penalties caused by ice formations on various airfoils*. Technical Note D-2166, National Aero-

	Segment i									
	1 / 20	2 / 19	3 / 18	4 / 17	5 / 16	6 / 15	7 / 14	8 / 13	9 / 12	10 / 11
$k^i_{C_{L0}}$	0.21201	0.19140	0.04382	−0.05401	−0.08956	−0.11607	−0.12817	−0.13397	−0.14374	−0.05904
$k^i_{C_{L\alpha,\mathrm{WB}}}$	−0.24934	−0.26912	−0.24910	−0.21078	−0.17369	−0.16700	−0.16903	−0.15869	−0.12378	−0.05569
$k^i_{C_{D0}}$	0.52586	0.47511	0.35921	0.24237	0.15032	0.09803	0.06483	0.03718	0.01488	0.04313
$d^i_{k_1}$	−0.05730	−0.05288	−0.03536	−0.02347	−0.00928	−0.00505	−0.00419	−0.00714	−0.00244	0.02295
$k^i_{k_2}$	4.14728	1.81220	1.74388	1.14707	0.62762	0.63235	0.67946	0.72906	0.89423	0.32086
$k^i_{\frac{\partial C_D}{\partial \bar{X}}}$	−0.48488	0.30413	0.20761	0.20098	0.22990	0.23328	0.33554	0.56470	0.21009	−0.02237
$k^i_{\alpha^*}$	−0.27097	−0.29210	−0.31879	−0.32208	−0.32543	−0.32986	−0.33705	−0.34259	−0.36263	−0.34640
$k^i_{c_1}$	0.37557	0.00000	0.94870	0.93992	0.62499	1.07812	2.40925	4.01841	4.34672	1.57112

Table 5: Estimated Δ-model parameters ($N = 20$)

nautics and Space Administration (NASA), Washington, D.C., USA, Februar, 1964.

[6] Broeren, Andy P.; Whalen, Edward A.; Busch, G. T. and Bragg, Michael B.: *Aerodynamic Simulation of Runback Ice Accretion*. Journal of Aircraft, Vol. 47, No. 3, pp. 924–939, May-June, 2010.

[7] Ranuado, Richard J.; Batterson, J. G.; Reehorst, A. L.; Bond, T.H. and O'Mara, T. M.: *Determination Of Longitudinal Aerodynamic Derivatives Using Flight Data From An Icing Research Aircraft*. 27th AIAA Aerospace Science Meeting, Reno, Nevada, USA, January 9th - 12th, 1989. American Institute of Aeronautics and Astronautics, Inc. (AIAA), Paper No. AIAA 89-0754.

[8] Ratvasky, Thomas P. and Ranuado, Richard J.: *Icing Effects on Aircraft Stability and Control Determined from Flight Data. Preliminary Results*. 31st AIAA Aerospace Science Meeting and Exhibit, Reno, Nevada, USA, January 11th - 14th, 1993. American Institute of Aeronautics and Astronautics, Inc. (AIAA), Paper No. AIAA 93-0398.

[9] Lee, Sam; Barnhart, Billy P. and Ratvasky, Thomas P.: *Dynamic Wind-Tunnel Testing of a Sub-Scale Iced S-3B Viking*. AIAA Atmospheric and Space Environments Conference, Toronto, Ontario Canada, August 2th - 5th, 2010. American Institute of Aeronautics and Astronautics, Inc. (AIAA), Paper No. AIAA 2010-7986.

[10] Gingras, David R.: *Requirements and Modeling of In-flight Icing Effects for Flight Training*. AIAA Modeling And Simulation Technologies (MST) Conference, Boston, Massachusetts, USA, August 19th - 22th, 2013. American Institute of Aeronautics and Astronautics, Inc. (AIAA), Paper No. AIAA 2013-5075.

[11] Bragg, Michael B.; Hutchison, Tim; Merret, Jason; Oltman, R. and Pokhariyal, Davesh: *Effect of Ice Accretion on Aircraft Flight Dynamics*. 38th AIAA Aerospace Science Meeting and Exhibit, Reno, Nevada, USA, January 10th - 13th, 2000. American Institute of Aeronautics and Astronautics, Inc. (AIAA), Paper No. AIAA 2000-0360.

[12] Brown, Anthony P.: *Negative Speed Stability, a Factor in Transport Airplane Icing Upsets*. 20th AIAA Applied Aerodynamics Conference, St. Louis, Missouri, USA, June 24th - 26th, 2002. American Institute of Aeronautics and Astronautics, Inc. (AIAA), Paper No. AIAA 2002-3051.

[13] Whalen, Edward A.; Lee, Sam; Bragg, Michael B. and Ratvasky, Thomas P.: *Characterizing the Effect of Ice on Aircraft Performance and Control from Flight Data*. 40th AIAA Aerospace Sciences Meetings and Exhibit, Reno, Nevada, USA, January 14th - 17th, 2002. American Institute of Aeronautics and Astronautics, Inc. (AIAA), Paper No. AIAA 2002-0816.

[14] Deters, Robert W.; Dimock, Glen A. and Selig, Michael S.: *Icing Encounter Flight Simulator*. Journal of Aircraft, Vol. 43, No. 5, pp. 1528–1537, September, 2006.

[15] Lampton, Amanda and Valasek, John: *Prediction of Icing Effects on the Dynamic Response of Light Airplanes*. Journal of Guidance, Control, and Dynamics, Vol. 30, No. 3, pp. 722–732, May-June, 2007.

[16] Ratvasky, Thomas P.; Barnhart, Billy P.; Lee, Sam and Cooper, Jon: *Flight Testing an Iced Business Jet for Flight Simulation Model Validation*. 45st AIAA Aerospace Science Meeting and Exhibit, Reno, Nevada, USA, January 8th - 11th, 2007. American Institute of Aeronautics and Astronautics, Inc. (AIAA), Paper No. AIAA-2007-0089.

[17] Jategaonkar, Ravindra V.: *Flight Vehicle System Identification - A Time Domain Methodology: Second Edition*, volume 245 of *Progress in Astronautics and Aeronautics*. American Institute of Aeronautics and Astronautics, Inc., 1801 Alexander Bell Drive, Reston, Virginia 20191, USA, 2015.

[18] Deiler, Christoph: *Time Domain Output Error System Identification of Iced Aircraft Aerodynamics*. Deutscher Luft- und Raumfahrtkongress, Rostock, September 22th - 24th, 2015. Deutsche Gesellschaft für Luft- und Raumfahrt (DGLR).

[19] Deiler, Christoph: *Aerodynamic Modeling, System Identification and Analysis of Iced Aircraft Configurations*. AIAA Aviation Forum and Exibition, Washington D.C., USA, June 13th - 17th, 2016. American Institute of Aeronautics and Astronautics, Inc. (AIAA).

[20] Ruff, G.A. and Berkowitz, B.M.: *Users Manual for the NASA Lewis Ice Accretion Prediction Code (LEWICE)*. Technical Report NASA CR-185129, NASA, 1990.

[21] Foss Van Zante, J.: *A Database of Supercooled Large Droplets Ice Accretions*. Technical Report NASA/CR – 2007-215020, NASA, 2007.

[22] Ghenai, C and Gin, C. X.: *Verification and Validation of NASA LEWICE 2.2 Icing Software Code*. Journal of Aircraft, Vol. 43, No. 5, pp. 1253–1258, September-Oktober, 2006.

[23] Gerhold, Thomas: *Overview of the Hybrid RANS Code TAU, MEGAFLOW - Numerical Flow Simulation for Aircraft Design*. Notes on Numerical Fluid Mechanics and Multidisciplinary Design, Vol. 89, pp. 81–92, 2005.

[24] Menter, F. R.: *Two-Equation Eddy-Viscosity Turbulence Models for Engineering Applications*. AIAA-Journal, Vol. 32, No. 8, pp. 1598–1605, August, 1994.

[25] Knopp, Tobias; Eisfeld, Bernhard and Bartolome Calvo, Javier: *A new extension for k-ω turbulence models to account for wall roughness*. International Journal of Heat and Fluid Flow, Vol. 30, No. 1, pp. 54–65, February, 2009.

[26] CentaurSoft, *CENTAUR Software*. retrieved June, 2016, http://www.centaursoft.com.

[27] Mönnich, Wulf: *Ein 2-Punkt-Aerodynamikmodell für die Identifizierung*. Symposium 'Systemidentifizierung in der Fahrzeugdynamik'. DFVLR Mitteilung 87-22, Paper No. 3.1, 1987, in German.

[28] Fischenberg, Dietrich and Jategaonkar, Ravindra V.: *Identification of Aircraft Stall Behavior from Flight Test Data*. RTO - MP - 11. Paper No. 17, March, 1999.

[29] Jategaonkar, Ravindra: *Identification of the Aerodynamic Model of the DLR Research Aircraft ATTAS from Flight Test Data*. Deutsche Forschungsanstalt für Luft- und Raumfahrt e. V. (DLR), Köln, September, 1990.

[30] Fischenberg, Dietrich: *Identification of an unsteady aerodynamic stall model from flight test data*. AIAA Atmospheric Flight Mechanics Conference, pages 138–146, Baltimore, Maryland, USA, August 7th - 10th, 1995. American Institute of Aeronautics and Astronautics, Inc. (AIAA), Paper No. AIAA 95-3438-CP.

[31] Seher-Weiß, Susanne: *FitlabGui - A Versatile Tool for Data Analysis, System Identification and Helicopter Handling Qualities Analysis*. 42nd European Rotorcraft Forum, Lille, France, 5th - 8th September, 2016.

[32] Sommerwerk, Hannah; Horst, Peter and Bansmer, Stephan: *Studies on Electro Impulse De-Icing of a Leading Edge Structure in an Icing Wind Tunnel*. AIAA Aviation Forum and Exibition, Washington D.C., USA, June 13th - 17th, 2016. American Institute of Aeronautics and Astronautics, Inc. (AIAA).

[33] Steiner, Jan: *Development of a 2D ice accretion computational method*. Deutscher Luft- und Raumfahrtkongress, Braunschweig, September 13th - 15th, 2016. Deutsche Gesellschaft für Luft- und Raumfahrt (DGLR).